Carbohydrate Polymers 89 (2012) 1222–1231

Contents lists available at SciVerse ScienceDirect

Carbohydrate Polymers

journal homepage: www.elsevier.com/locate/carbpol

Combined QCMD and AFM studies of lysozyme and poly-L-lysine–poly-galacturonic acid multilayers

Marta Westwood*, Andrew R. Kirby, Roger Parker, Victor J. Morris

Institute of Food Research, Norwich Research Park, Colney, Norwich NR4 7UA, UK

ARTICLE INFO

Article history:
Received 26 September 2011
Received in revised form 31 January 2012
Accepted 31 March 2012
Available online 6 April 2012

Keywords:
Polyelectrolytes
Multilayers
Assembly
AFM
QCMD

ABSTRACT

A quartz crystal microbalance with dissipation monitoring (QCMD) has been used to monitor the adsorption and structure of lysozyme monolayers and multilayers, and poly-L-lysine (PLL)–polygalacturonic acid (PGalA) multilayers at a solid–liquid interface using freshly-cleaved mica as a substrate. QCMD measurements were complemented with atomic force microscopy (AFM). AFM images revealed that lysozyme formed incomplete monolayers and provided a basis for calculation of the thickness of the protein film. Comparative studies of adsorption onto standard and mica-coated quartz crystals showed higher areal mass adsorption and a longer-time adsorption process for mica-coated quartz crystals. Simultaneous AFM images and QCMD data were obtained for lysozyme, linear PLL–PGalA and 7 nm PLL dendrimer-PGalA multilayers. The layer-by-layer deposited multilayer films exhibited viscoelastic properties and their growth followed a non-linear regime, associated with the PLL diffusion in and out of the film formation for linear PLL–PGalA films. For the PLL 7 nm dendrimer-PGalA films the AFM images revealed marked changes in surface roughness during layer by layer deposition: these changes influence the interpretation of the QCMD data and provide additional information on the growth and structure of the multilayers.

1. Introduction

The quartz crystal microbalance with dissipation monitoring (QCMD) is a valuable tool used for characterising adsorption of biological molecules onto surfaces (Halthur, Arnebrant, Macakova, & Feiler, 2010; Hemmersam, Rechendorff, Besenbacher, Kasemo, & Sutherland, 2008; Hook et al., 2001; Johannsmann, Reviakine, Rojas, & Gallego, 2008) and for studying self-assembly of layers (Alves, Picart, & Mano, 2009; de Kerchove & Elimelech, 2007) or multilayers (Bieker & Schonhoff, 2010; Garg, Heflin, Gibson, & Davis, 2008; Kesimer & Sheehan, 2008; Kett et al., 2009; Laos, Parker, Moffat, Wellner, & Ring, 2006; Macakova, Yakubov, Plunkett, & Stokes, 2010) at surfaces. The technique allows monitoring of the dynamic assembly of such processes and provides both qualitative and quantitative information on the formed structures. Deposition is accompanied by a change in the resonant frequency of the quartz crystal. Thus the formation of the film can be monitored and the value for the change in resonant frequency can be used to calculate the hydrated mass and, assuming a density, a thickness of the deposited film. These calculations model the adsorbed molecules as a homogeneous, rigid elastic layer. The dynamic nature of the preparation of monolayers and multilayers is such that the layers are unlikely to be homogeneous and, as subsequent layers are deposited, the resultant formed structures are likely to be viscoelastic in nature. Thus it would be useful to have direct structural information on the deposited layers in order to complement analysis of the QCMD data. Probe microscopy is an ideal technique for visualising structures deposited onto substrates and there have been several attempts to combine QCMD and probe microscopy measurements (Borovsky, Mason, & Krim, 2000; Bund, Schneider, & Dehnke, 2002; Choi, Friedt, Frederix, Campitelli, & Borghs, 2002; Heim & Johannsmann, 2007; Iwata, Kawaguchi, Aoyama, & Sasaki, 1997; Johannsmann et al., 2008; Kautek, Dieluweit, & Sahre, 1997; Rojas, Gallego, & Reviakine, 2008) either on quartz crystals or material deposited on such crystals. Studies of protein adsorption on quartz crystals were made using fibrinogen (Choi et al., 2002) and ferritin (Johannsmann et al., 2008; Rojas et al., 2008) that are large enough proteins to be visible on the surface of the crystals. However, in general the gold-coated or silicon dioxide-coated surfaces of quartz crystals are rough in comparison with the size of most biomacromolecules. This limits the use of surface techniques such as atomic force microscopy (AFM) for visualising the molecular structures formed on adsorption. AFM is ideally suited for imaging biological molecules adsorbed onto atomically flat substrates such as freshly-cleaved hydrophilic mica or hydrophobic graphite surfaces. The technique can be used together with simulation

* Corresponding author. Tel.: +44 1753 534 655; fax: +44 1753 447 590.
E-mail addresses: marta.westwood@ucb.com (M. Westwood), andrew.kirby@ifr.ac.uk (A.R. Kirby), roger.parker@ifr.ac.uk (R. Parker), vic.morris@ifr.ac.uk (V.J. Morris).

0144-8617/$ – see front matter © 2012 Elsevier Ltd. All rights reserved.
http://dx.doi.org/10.1016/j.carbpol.2012.03.097

studies to characterise and model biopolymer adsorption onto surfaces (Kim, Blanch, & Radke, 2002; Pellenc, Bennett, Green, Sperrin, & Mulheran, 2008). The nature of the deposited layer is sensitive to the roughness and the physicochemical nature of the substrate: the impact of the surface roughness on QCMD response has been discussed in some detail by different research groups (Daikhin et al., 2002; Jordan & Fernandez, 2008; Martin, Frye, Ricco, & Senturia, 1993). Recently, Vörös and co-workers investigated how the morphology of layer-by-layer deposited polyelectrolyte multilayers is affected by the physical properties of the supporting substrate (Guillaume-Gentil et al., 2011). Hence it would be useful to carry out complementary QCMD and AFM studies on deposition onto mica surfaces.

In this article these studies have been carried out using mica discs in the QCMD apparatus and also mica-coated quartz crystals, prepared by a modification of the methods developed by Richter and Brisson (2004). The latter approach has proved successful in providing new insights into the assembly and properties of supported lipid bilayers (Richter, Berat, & Brisson, 2006; Richter & Brisson, 2005; Richter, Him, Tessier, Tessier, & Brisson, 2005). In the present studies the combined use of QCMD and AFM has provided new information on the structure of lysozyme monolayers and multilayers, and also on the assembly and structure of poly-L-lysine (PLL)–polygalacturonic acid (PGalA) multilayers.

2. Materials and methods

2.1. Materials

Hens egg lysozyme (L6876) was obtained from Sigma–Aldrich Ltd. (Gillingham, UK). The reagents were analytical grade and used without further purification. The lysozyme solutions were prepared by dissolving the biopolymer at a concentration of 0.6 mg mL^{-1} in 150 mM pH 7.5 phosphate buffer containing 30 mM NaCl (PBS). Poly-L-lysine (PLL) dendrimers (Generation G3; diameter 7 nm) were obtained from Colcom, France, linear poly-L-lysine (P6516; mean degree of polymerisation, 70) from Sigma Aldrich, UK and polygalacturonic acid (PGalA) from Fluka, Biochemika. The PLL dendrimers and PGalA solutions were also prepared at a concentration of 0.6 mg mL^{-1} in 10 mM PBS.

Prior to deposition the substrate surfaces were cleaned using a UV-Ozone chamber (Bioforce Nanosciences, Inc., IA, USA), then rinsed thoroughly with water and dried with N_2. Mica discs of diameters 9.9 mm and 14 mm were purchased from Agar Scientific, UK.

2.2. Preparation of mica-coated QCMD sensors

The method for attaching 10 mm mica discs to standard QCMD chips was broadly based on a procedure developed by Richter and Brisson (2004). It is essential to bond the mica rigidly and evenly across the entire working surface of the chip, otherwise its resonant properties will be altered dramatically and it will be unusable for mass detection. Additionally the combined mass of mica and glue (Loctite 326, Henkel Ltd., UK) added to the QCMD chip during the procedure must be kept to an absolute minimum. Failure to do this will reduce its resonant frequency to a level outside the detectable range of the instrument, and secondly the Q-factor of the chip will be reduced so that the measurements are insensitive to small changes in mass of the deposited material. In order to reliably pipette a small droplet (1 μL) of glue, and to ensure that it spreads evenly, it was necessary to dilute it with chloroform to a final concentration of 20%. With practice it was possible to optimise the quantity and concentration of the glue in order to cover the region between the mica and the chip without spilling out over the electrodes. The mica-coated QCMD chip composite was clamped between two glass slides using a bulldog clip and then heated to 50 °C overnight in an oven. Final curing was performed by exposure to UV light from a UV-Ozone chamber for 15 min. Finally, the mica was cleaved with Scotch tape (3 M) to expose a clean and even surface and to substantially reduce its thickness. This presented a considerable practical challenge and was the main limitation on the use of coated crystals: it was important to avoid damaging the chip or removing so much mica so that the thin glue layer was exposed. Ultimately only about 20% of the mica-coated QCMD chip composites were usable. The number of layers cleaved from the mica could be estimated by monitoring the mass of the mica-crystal composite. Cleavage of mica layers was continued until a workable resonant frequency was achieved, typically ~4.94 MHz.

2.3. Quartz crystal microbalance with dissipation monitoring (QCMD)

QCMD measurements were performed using a D300 QCMD (Q-Sense AB, Västra Frölunda, Sweden) with a QAFC 302 axial flow measurement chamber as described elsewhere (Rodahl, Hook, Krozer, Brzezinski, & Kasemo, 1995). Silicon dioxide coated AT-cut quartz crystals sandwiched between gold electrodes (QSX-303) as supplied by Q-Sense AB and mica-coated QCMD sensors were used as the substrate. The QCMD sensor was placed in the measurement chamber and an AC voltage applied to excite the fundamental resonant frequency of the crystal (average value ~4.96 MHz) and its overtones (n = 3, 5, 7), or the modified crystal (average value ~4.94 MHz) and its 3rd overtone. All measurements were performed in a liquid environment at 20 °C in the batch exchange mode. Additional experiments were carried out with the QCMD sensor replaced by a 14 mm diameter mica disc. The discs are thinner than the normal QCMD sensor. In order to prevent leakage from the chamber the mica discs were placed on top of a 'dummy' QCMD sensor unconnected to the mica disc and used purely as a spacer.

The adsorption of lysozyme, poly-L-lysine dendrimers, poly-L-lysine-PGalA and poly-L-lysine dendrimer-PGalA multilayers was followed in real-time by monitoring changes in the oscillation frequencies (Δf_n) of the crystal. A decrease in oscillation frequency indicates the adsorption of mass onto the QCMD sensor. If the mass is deposited evenly, and forms a rigid elastic layer, then the negative frequency changes are proportional to the hydrated mass deposited (Δm) as described by the Sauerbrey equation (Sauerbrey, 1959).

$$\Delta m = \frac{-C\Delta f_n}{n} \quad (1)$$

where C is the mass sensitivity constant (C = 17.7 ng cm^{-2} Hz^{-1} for a 5 MHz crystal (Hook et al., 2001) and Δf_n the frequency shift of the nth overtone). For standard QCMD sensors the average fundamental frequency is ~4.96 MHz. Thus C = 17.9 ng cm^{-2} Hz^{-1}. For the mica-coated QCMD sensors the average fundamental frequency was found to be ~4.94 MHz (C = 18.012 ng cm^{-2} Hz^{-1}). In practice the correction to the mass sensitivity constant for the change in resonance frequency leads to small changes in the calculated adsorbed mass. The solutions were filtered through 0.2 μm filters before being introduced into the QCMD cells.

In the case of polyelectrolyte adsorption additional information, regarding the viscoelastic properties of the films were extracted from measurements of dissipation. The dissipation factor D is defined by:

$$D = \frac{E_{\text{dissipated}}}{2\pi E_{\text{stored}}} \quad (2)$$

where $E_{dissipated}$ is the energy dissipated during one oscillation and E_{stored} is the energy stored in the oscillating system.

For rigidly attached species no change in dissipation will be observed as a function of adsorption. However, for an adsorbed viscoelastic layer, the energy dissipated through the layer will increase. Therefore, by observing the change in dissipation (ΔD), a qualitative measure of the relative stiffness of an adsorbed layer may be determined. As the Sauerbrey equation may lead to mass underestimation, due to the viscoelastic properties of an adsorbed film, the thickness and the viscous and shear modulus components of the adsorbed film were obtained by fitting theoretical representations based on the Voigt model with the Q-Tools software from Q-Sense AB. Since the bulk solution was dilute, its density ($\rho_s \approx 1000\,kg\,m^{-3}$) and viscosity ($\eta_s \approx 1\,mPa\,s$) were taken to be those of water. The effective density (ρ_{eff}) used to describe the layer was $1100\,kg\,m^{-3}$.

For imaging by AFM the QCMD sensors, mica-coated QCMD sensors and the free mica discs were transferred to and from the AFM under liquid in order to avoid artifacts induced by drying and rehydrating the samples. Deposition onto isolated mica discs could not be monitored directly and was carried out under identical conditions to those previously monitored using the normal QCMD chip. Feasibility studies were made using simultaneous deposition onto QCMD chips and mica discs using series or parallel arrangement of two QCMD chambers: the mica-coated QCMD chip was used to monitor deposition and the mica disc to image the deposited layers.

2.4. Atomic force microscopy (AFM)

The instrument used was an MFP-3D BIO (Asylum Research, Santa Barbara CA). Images were recorded in AC mode both in air and under buffer. In air, Olympus Corp. (Tokyo, Japan) AC160TS cantilevers were used with a spring constant of $42\,N\,m^{-1}$. Under buffer, Olympus AC40TS 'BioLever Mini' cantilevers were used with a spring constant of $0.1\,N\,m^{-1}$. In this case the cantilever was operated at just below the second Eigen frequency. Instead of a liquid cell the sample was attached to a PTFE printed slide (Electron Microscopy Sciences, Hatfield, PA, USA) as the tight meniscus formed by the liquid was found to enhance the identity of the various Eigen frequencies. The gray scale in the images is linear and the amplitude (black to white) is given as dz.

Table 1
Reduced frequency shift, Sauerbrey hydrated mass and thickness of an adsorbed lysozyme monolayer measured using QCMD with standard and mica-coated quartz crystal sensors. Lysozyme adsorbed from $0.6\,mg\,mL^{-1}$ solution in 150 mM PBS.

	Standard sensor	Mica-coated sensor
$\Delta f_n/n$ (n = 1, 3) (Hz)	8.5–12.5 (average 10.5)	12–20 (average 14)
Hydrated mass ($ng\,cm^{-2}$)	160–220 (average 186)	210–350 (average 250)
Thickness assuming $\rho = 1100\,kg\,m^{-3}$ (nm)	1.52–2.1 (average 1.8)	2.0–3.37 (average 2.4)

3. Results and discussion

3.1. Lysozyme adsorption onto silicon dioxide and mica surfaces

In order to assess the potential of the combined use of QCMD and AFM the two techniques have been used to monitor surface deposition of a well-characterised globular protein lysozyme. Table 1 shows the QCMD data for a lysozyme monolayer formed on a silicon dioxide-coated quartz crystal. In replica experiments there was variability in the frequency shift at the saturated value, corresponding to formation of a monolayer, resulting in variability in the calculated hydrated areal mass and layer thickness (Table 1). In order to understand this variability the monolayer structures were imaged by AFM. Mica discs were placed on top of quartz crystals in the QCMD apparatus and lysozyme monolayers were deposited onto these discs under the same experimental conditions. Fig. 1a shows an image of the protein structure formed on the mica disc. The deposits show a protein network which contains areas of bare mica and a few aggregates. The holes in the network correspond to ~30% of the total area. The measured height of the monolayer from the height profiles suggests a thickness of ~1.8 nm. Within the protein region of the monolayer the surface roughness corresponds to ~540 pm. These images suggest that the variability in the observed saturation frequency shift is due to the heterogeneity of the structure and the consequent variable surface coverage. Possible reasons for the variability in the surface coverage are suggested by AFM and simulation studies of the adsorption of lysozyme onto mica (Kim et al., 2002; Pellenc et al., 2008). These studies suggest that, on adsorption, the proteins undergo conformational changes due to protein–surface interactions that expose hydrophobic regions that,

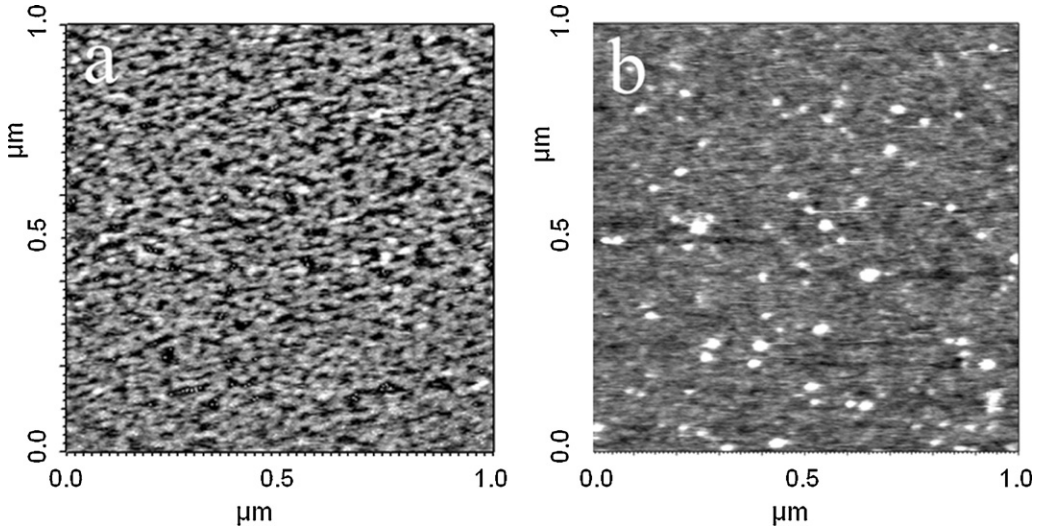

Fig. 1. Topographical AFM images of a lysozyme deposited onto freshly-cleaved mica (a) monolayer, image size: 1 μm × 1 μm, *dz* (height scale black to white) 3 nm and (b) 3 layer lysozyme film, image size: 1 μm × 1 μm, *dz* = 1.1 nm.

in turn, can interact with similar exposed residues on other surface-adsorbed proteins. Such interactions lead to cluster formation and the clusters can then diffuse on the surface. The slow surface diffusion and distribution of the clusters on the surface will influence subsequent adsorption and complete monolayer coverage can take hours to be achieved, although the timescales will be dependent on the protein concentration and conditions (pH, ionic strength). For the present studies, and for reported studies of the adsorption of lysozyme onto silicon dioxide by dual polarisation interferometry (Lu, Swann, Peel, & Freeman, 2004) and silicon dioxide by QCMD (Lundin, Elofsson, Blomberg, & Rutland, 2010; Messina, Satriano, & Marletta, 2009), the timescales for adsorption are too short to ensure complete monolayer coverage. As such the structures are non-equilibrium structures: it is then not possible to assume uniform coverage in order to compare the calculated mass per unit area or the layer thickness, even when deposition has been made at the same protein concentration and under nominally the same experimental conditions. Thus AFM data provides information on surface coverage giving a fuller characterisation of the adsorption process.

Fig. 1b shows AFM images of a multilayer structure formed by sequential layer by layer deposition of 3 layers of lysozyme onto the substrate. The surface of the multilayer is fairly flat (surface roughness ~186 pm) with a few defect structures and (bright) protrusions of heights between 1.5 and 3.0 nm, probably due to adsorption of individual proteins or small protein aggregates onto the surface of the multilayer. This is consistent with previous AFM and simulation studies which suggest the formation of discrete layers before a new layer begins to form (Kim et al., 2002; Pellenc et al., 2008). The present and previous studies suggest that surface adsorption is irreversible: removal of the protein in the aqueous phase or washing does not cause the protein to desorb from the surface. In these studies the QCMD data is for lysozyme deposited onto silicon dioxide-coated quartz crystals and the AFM data is for lysozyme deposited onto freshly-cleaved mica. Table 1 also shows QCMD data for lysozyme adsorbed onto mica-coated quartz crystals; the same pattern of adsorption was observed but the saturation values indicated a larger frequency shift corresponding to higher calculated mass and layer thickness. Clearly the nature of the substrate affects the structure of the adsorbed film. The level of variability between replica experiments was also similar to that observed with the silicon dioxide-coated quartz crystals, consistent with the observed heterogeneous structure.

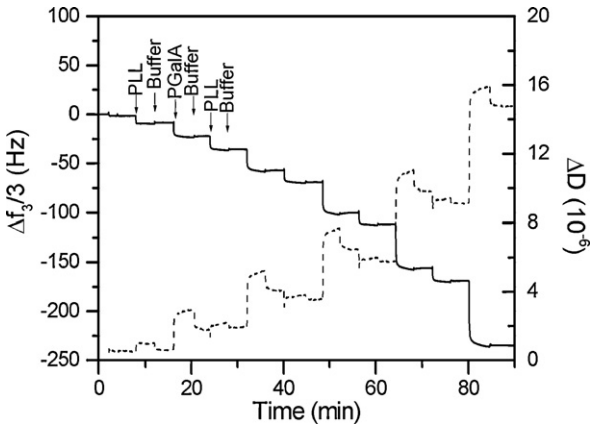

Fig. 2. QCMD response data, $\Delta f_3/3$ (—) and ΔD_3 (- - -) obtained during the layer-by-layer deposition of a 10-layer linear PLL–PGalA film.

3.2. PLL–PGalA multilayer deposition onto mica surfaces

The above experiments demonstrate that it is possible to obtain both QCMD and AFM data on the adsorption of monolayers and multilayers on mica. For these experiments the measurements were made in separate experiments under similar conditions. It would be possible to collect such data under exactly the same conditions by connecting two QCMD cells in a series or parallel configuration, with one cell containing a dummy mica disc sitting atop of a quartz crystal, and the other cell containing a mica-coated quartz crystal. The latter cell can then be used to obtain QCMD measurements for adsorption onto mica and the former cell for AFM imaging of the layer structure formed on the mica. This approach has been illustrated by studies on linear PLL–PGalA multilayers. Previous real-time QCMD studies on the formation of PLL–PGalA multilayer structures have shown that, due to the strong electrostatic interactions between linear PLL and PGalA, adsorption of each biopolymer occurs rapidly, with the plateau region being reached after approximately 2 min (Westwood, Noel, & Parker, 2010). Fig. 2

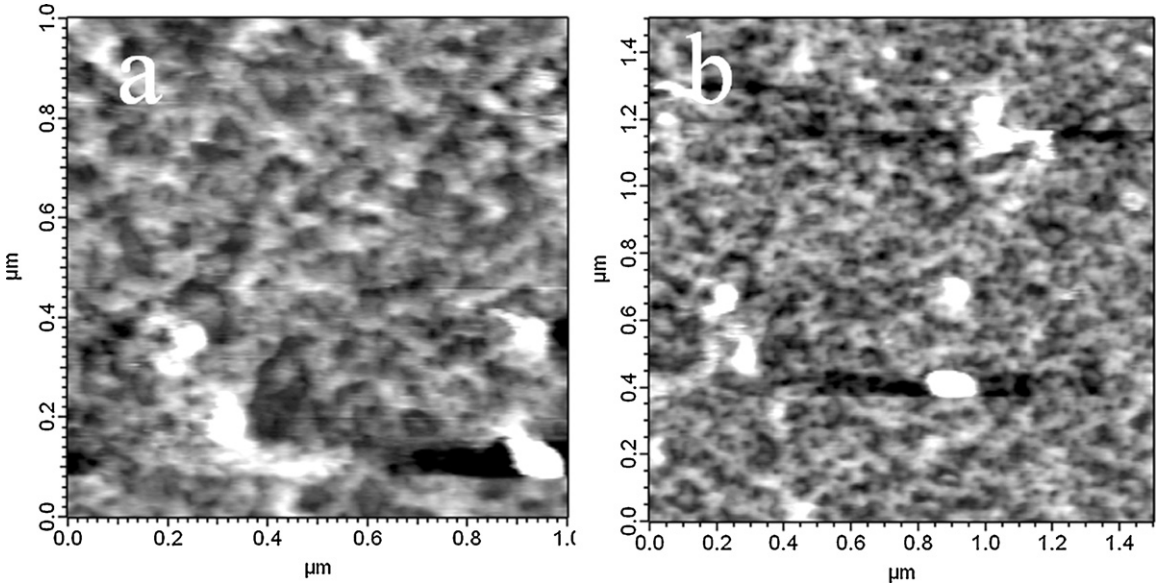

Fig. 3. Topographical AFM images of a 10 layer linear PLL–PGalA multilayer film deposited onto a freshly-cleaved mica disc under the same experimental conditions as that shown in Fig. 2. (a) Image size 1 µm × 1 µm, dz = 18.5 nm and (b) image size 1.5 µm × 1.5 µm, dz = 20 nm.

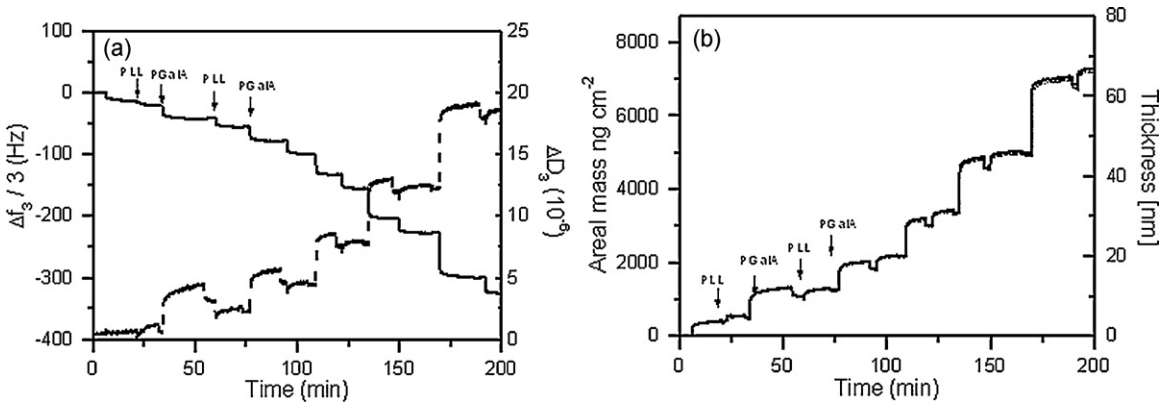

Fig. 4. Changes in (a) $\Delta f_3/3$, (b) areal mass and thickness collected for linear PLL–PGalA 10-layers deposited in parallel onto mica-coated quartz crystals and mica discs.

shows conventional QCMD data for the formation of a 10-layer PLL–PGalA structure in real time. The PLL adsorption was indicated by a rapid decrease in $\Delta f_3/3$ with a minimal increase in ΔD_3. In contrast, during the PGalA deposition, the decrease in $\Delta f_3/3$ was accompanied by a significant increase in ΔD_3. The PLL–PGalA multilayer assembly process was found to be almost irreversible, with minor amounts of non-absorbed polyelectrolyte being removed upon rinsing with the buffer solution, following adsorption of each polymer layer. The total change in frequency accompanying a 10-layer assembly was observed to be approximately -220 ± 15 Hz. The decrease in $\Delta f_3/3$ is a measure of the mass adsorption at each deposition step. It is well known that the QCMD response is sensitive to the viscoelastic properties of any mass coupled to the quartz crystal, including adsorbed biopolymers, water, and salt coupled to the biopolymer layer. As the multilayer films tend to behave as viscoelastic, rather than purely elastic films, the information regarding the viscoelastic properties of the PLL–PGalA multilayers was extracted from the changes in frequency and dissipation observed during the multilayer assembly. The total hydrated mass of 4900 ± 450 ng cm^{-2} was estimated using the Voigt-based model. The film thickness was estimated, assuming a homogeneous viscoelastic film, characterised by a shear viscosity, a shear modulus, and an effective density. The solution viscosity, η_s, and density, ρ_s values for the films were taken to be 1 mPa s and 1000 kg m^{-3}, respectively, and the effective film density ρ_{eff} was assumed to be 1100 kg m^{-3}. The QCMD results showed that the formed multilayer film exhibited viscoelastic properties and that the multilayer growth followed a non-linear regime due to PLL diffusion in and out of the multilayer during film formation.

AFM images of the 10 layer linear PLL–PGalA multilayer were obtained by depositing the multilayer onto a freshly-cleaved mica disc placed on top of a quartz crystal in the QCMD cell. The deposition conditions were the same as those used for the data shown in Fig. 2. After deposition the free mica discs were transferred to the AFM under liquid, in order to avoid artifacts induced by drying and re-hydrating the samples. The hydrated multilayer was then imaged in AC mode. Fig. 3 shows topographical AFM images of the 10 layer film deposited on freshly-cleaved mica. The AFM images revealed a relatively homogeneous fibrous network containing a few large aggregates and with a surface roughness (root mean square, RMS) of 4.3 nm. Although every effort was made to ensure that the deposition time and the concentration of the solutions used to assemble the 10-layer PLL–PGalA film on the QCMD sensor (used for QCMD measurement) and on the mica disc (AFM measurement) were kept the same, it is known that the molecular adsorption is very sensitive to the nature of the surface. This has been shown to be true for deposition of lysozyme onto silicon dioxide-coated and mica-coated quartz crystals. Experimental

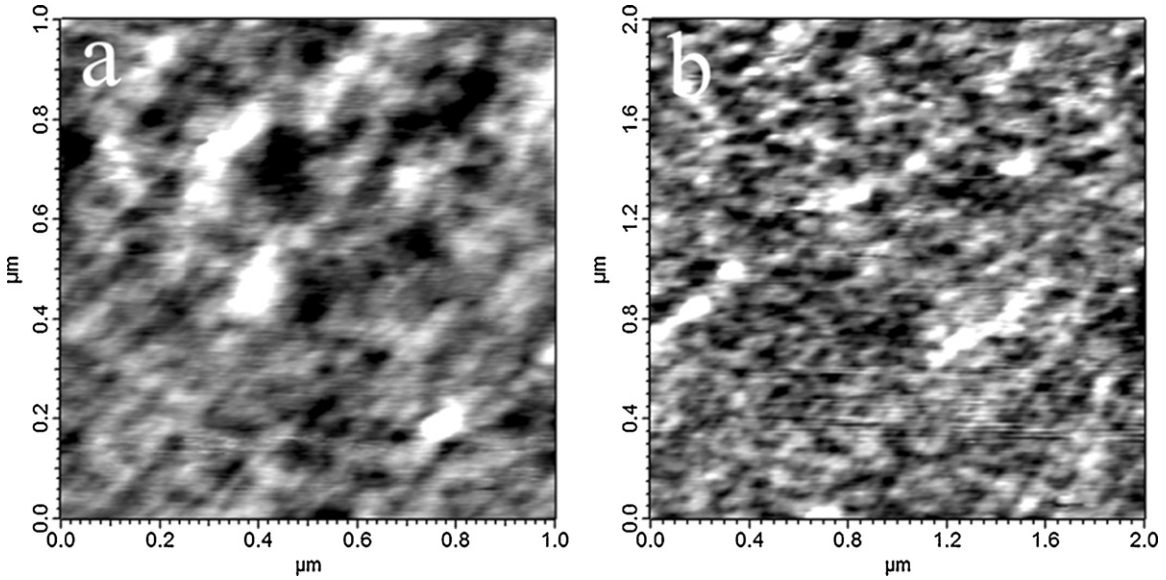

Fig. 5. AFM topography images of a linear PLL–PGalA 10-layer film deposited onto freshly-cleaved mica discs in the parallel chamber configuration. (a) Image size 1 μm × 1 μm, dz = 7.8 nm and (b) image size 2 μm × 2 μm, dz = 7.8 nm.

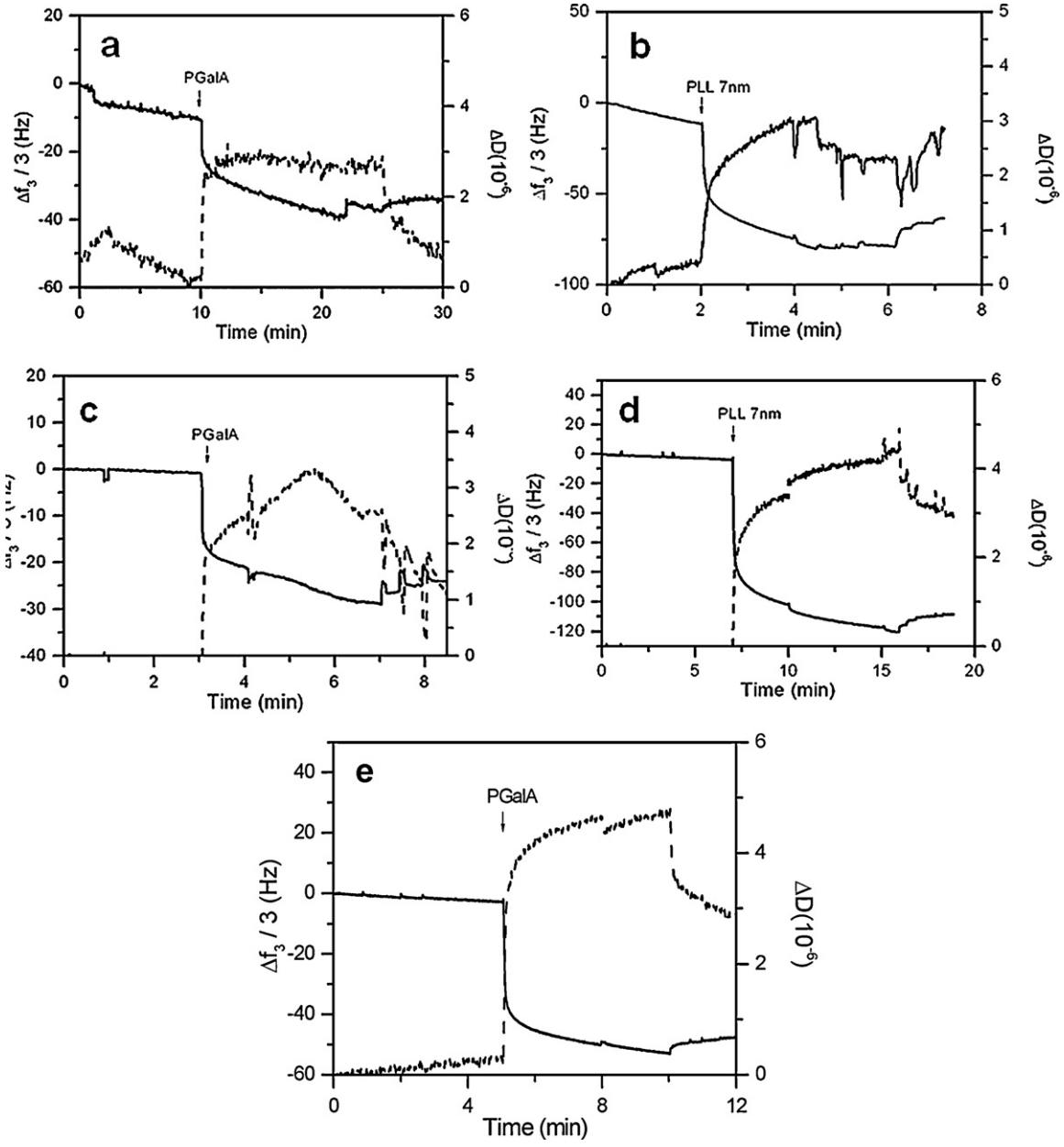

Fig. 6. Changes in $\Delta f_3/3$ and dissipation ΔD_3 measured with the QCMD during the deposition of a PLL 7 nm dendrimer-PGalA structure onto a linear PLL base layer after each deposition step. (a) 2 layer-film (with PGalA as the top layer), (b) a 3 layer-film (with the PLL 7 nm dendrimer as the top layer), (c) 4 layer-film (with PGalA as the top layer), (d) a 5 layer-film (with the PLL 7 nm dendrimer as the top layer), and (e) a 6 layer film (with PGalA as the top layer). Note that due to removal of the mica-coated quartz crystal for AFM measurements the changes in $\Delta f_3/3$ and dissipation ΔD_3 begin at zero for deposition of the next layer.

parameters such as flow rate and small differences in deposition conditions can influence significantly the formation and properties of the formed mono- or multilayer films. As shown for lysozyme even successive runs using the same deposition conditions can yield different calculated mass and thickness values for the films if the deposited films are heterogeneous in structure. In order to minimise differences in the experimental set up, and to obtain maximum information on the formed multilayer films, studies were therefore made using simultaneous deposition in identical flow chambers onto mica discs and onto a mica-coated quartz crystal, using the two cells connected in parallel or series configurations. This should provide identical deposition condition for both the mica and the mica-coated quartz crystals (on which QCMD data can be recorded).

Figs. 4 and 5 show the QCMD and AFM data for PLL–PGalA multilayers collected using a QCMD cell containing a mica-coated quartz crystal connected in parallel with a cell containing a mica disc. Fig. 4 shows the QCMD data ($\Delta f_3/3$ and ΔD_3) recorded during the formation of a 10-layer linear PLL–PGalA film on a mica-coated quartz crystal and the corresponding calculated values of the hydrated mass and layer thickness. The results show a continuous decrease in resonant frequency with each subsequent deposition step indicating the adsorption of biopolymers leading to a multilayer structure. Comparison of the QCMD data obtained using an ordinary QCMD sensor (Fig. 2) with data from the mica-coated QCMD sensor (Fig. 4) showed a good agreement, although the recorded values of $\Delta f_3/3$ (-320 Hz) and ΔD_3 (18×10^{-6}) are slightly higher for the mica-coated QCMD sensor. This is similar to what was observed for the adsorption of lysozyme and indicates the influence of the substrate structure. Furthermore it was observed that it took about twice as long to form the 10-layer PLL–PGalA film on the mica-coated QCMD sensor than on the ordinary QCMD sensor. These results

are encouraging and show that mica-coated quartz crystals can be used to monitor deposition of such large multilayer structures. Furthermore, it was also possible to clean the mica-coated quartz crystals, using the same procedures used for cleaning quartz crystals, suggesting that the mica-coated quartz crystals are re-usable. After these multilayers were formed and QCMD measurement was completed (Fig. 4), the structure formed on the mica disc (in the additional cell) was transferred under liquid and imaged in the hydrated state using AFM. Fig. 5 shows representative topographical AFM images for the deposit on the mica disc connected in parallel with the mica-coated quartz crystal. The images have been captured from equivalent positions near the centre of the samples in Figs. 3 and 5. The images obtained on the mica discs in parallel with the mica-coated quartz crystal are similar to those obtained previously in Fig. 3. They show a reasonably uniform structure with a surface roughness (RMS) of ~1.2 nm. These experiments demonstrate that it is possible to obtain simultaneous QCMD and AFM data on multilayer deposition onto mica. The experiments show that the time required to form the film on the mica is longer than for the standard quartz crystal surfaces and that a larger mass is deposited onto the mica surface.

3.3. Structural evolution of PLL–GalA multilayers formed on mica surfaces

For multilayers it would be useful to monitor the development of the film structure layer by layer. This can be done by depositing onto the mica disc, transferring the hydrated disc to the AFM, imaging the film and then transferring the disc back to the QCMD cell. Provided the sample is kept under liquid during the transfer and imaging process then it is possible to deposit another layer and repeat the process. An alternative is just to deposit onto a mica-coated quartz crystal and use this for both QCMD measurements and AFM imaging. This is possible if the transfer between QCMD cell and the AFM is done under liquid. The process is time-consuming but provides data on the same sample. This is likely to be important if the sample shows substantial heterogeneity during development of the multilayer structure. This was found to occur if multilayers are formed using a 7 nm PLL dendrimer rather than linear PLL. Fig. 6 shows the results of the QCMD data for this type of experiment. In order to clearly demonstrate the changes occurring to the multilayer structure at each deposition step, PLL 7 nm dendrimer, instead of the linear PLL was used for the

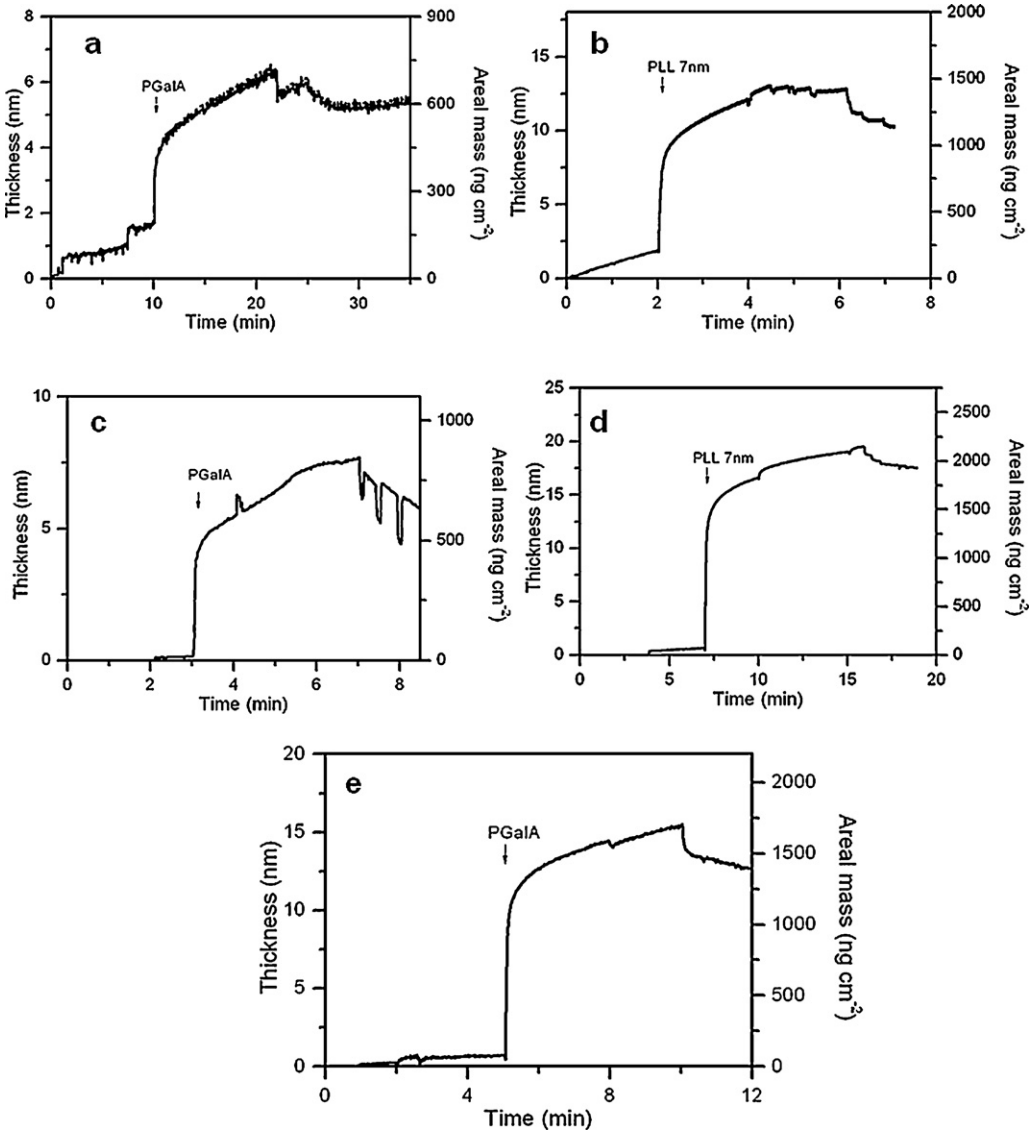

Fig. 7. Calculated changes in areal mass and thickness during the deposition of a PLL 7 nm dendrimer-PGalA structure onto a linear PLL base layer after each deposition step. (a) 2 layer-film (with PGalA as the top layer), (b) a 3 layer-film (with the PLL 7 nm dendrimer as the top layer), (c) 4 layer-film (with PGalA as the top layer), (d) a 5 layer-film (with the PLL 7 nm dendrimer as the top layer), and (e) a 6 layer film (with PGalA as the top layer).

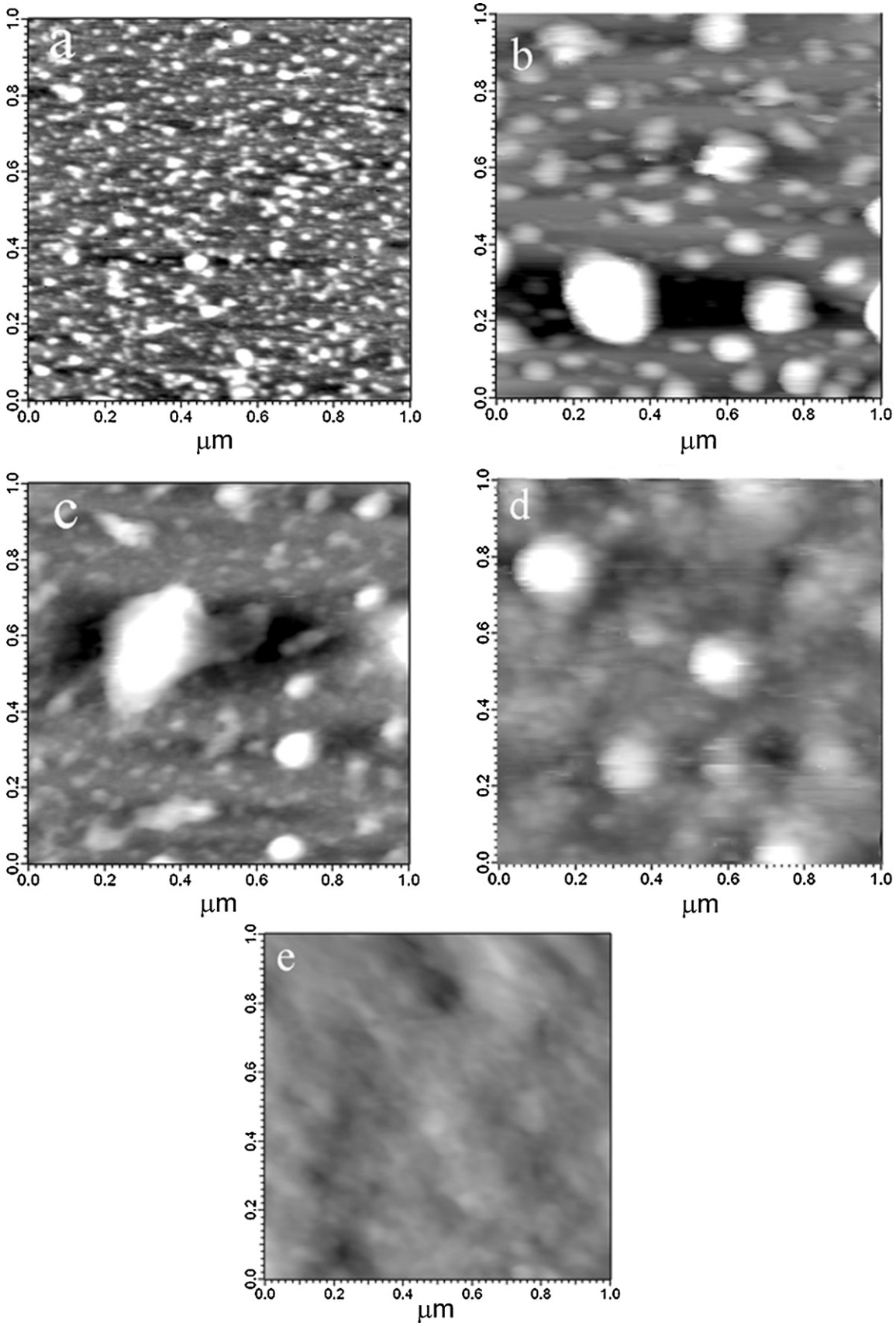

Fig. 8. AFM topography images showing the surface of a PLL 7 nm dendrimer-PGalA structure after various deposition steps onto an initial linear PLL layer. (a) 2 layer-film (with PGalA as the top layer), dz = 2.5 nm, (b) 3 layer-film (with PLL 7 nm dendrimer being the top layer), dz = 55 nm, (c) 4 layer-film (with PGalA being the top layer), dz = 16.5 nm, (d) 5 layer-film (with PLL 7 nm dendrimer being the top layer), dz = 53.7 nm, and (e) 6 layer film (with PGalA being the top layer), dz = 30 nm. Image sizes 1 μm × 1 μm.

multilayer assembly of PLL–PGalA films on the mica-coated QCMD sensor. Multilayer formation was monitored using both the QCMD and AFM techniques. As a precursor layer linear PLL was initially deposited onto a mica-coated QCMD sensor. Detailed studies were then made on multilayer assembly of PLL 7 nm dendrimer-PGalA, starting from the deposition of the 2nd PGalA layer, which was then followed by the deposition of PLL 7 nm dendrimer, and then successive alternative deposition until a total 6-layer film structure was fabricated. Fig. 6 shows the data for deposition of the 2nd–6th layers of the film and Fig. 7 shows the calculated areal mass at each deposition stage and the calculated change in film thickness.

Fig. 6a and b shows the changes in $\Delta f_3/3$ and ΔD_3, and Fig. 7a and b shows the associated total hydrated mass and the thickness of the 2nd PGalA layer. The QCMD results suggest that the deposition of the 2nd PGalA layer led to the formation of a 4.2 nm thick film with a total hydrated mass of 400 ng cm^{-2}. The corresponding AFM image of the bilayer structure (Fig. 8a) revealed formation of a relatively uniform structure containing small surface protrusions giving rise to a surface roughness (RMS) of 0.56 nm. The sample was then returned to the QCMD apparatus without allowing the sample to dry. Prior to deposition of a 3rd (PLL 7 nm dendrimer) layer the QCMD sensor was equilibrated with buffer. The deposition of PLL 7 nm dendrimer led to a decrease in $\Delta f_3/3$ of ~ -50 Hz (Fig. 6b). The observed small changes in dissipation suggested that the layer was relatively rigid, and the $\Delta f_3/3$ changes resulted in a hydrated mass of $\sim$950 ng cm^{-2} and a corresponding layer thickness of 8.5 nm (Fig. 7b). The calculated thickness was higher than the expected 7-nm associated with the diameter of the dendrimer. It suggests that PLL 7 nm dendrimer formed a monolayer, with aggregated areas leading to the higher thickness value. The AFM image (Fig. 8b), taken directly after deposition of the 3rd layer showed a rough layered structure containing globular protrusions. The images demonstrate the formation of PLL 7 nm dendrimer aggregates within the dendrimer layer adsorbed on the PGalA layer, which accounts for the increased surface roughness (RMS) values of 9.52 nm. Transfer of the sample back to the QCMD allowed deposition of the 4th (PGalA) layer which led to a decrease in $\Delta f_3/3$ of ~ -25 Hz, and the formation of a thinner, 6 nm layer containing an estimated hydrated mass of $\sim$650 ng cm^{-2} (Figs. 6c and 7c) The dissipation, which initially increased to 3×10^{-6} during the deposition of PGalA, then decreased to 1.5×10^{-6} following the rinse with buffer, indicating that the PGalA layer underwent a conformational changes resulting in the 'stiffening' of the adsorbed layer. The corresponding AFM image (Fig. 8c) showed observable structural changes associated with the deposition of the PGalA layer: the surface became smoother showing a lower surface roughness (RMS) of 5.67 nm and the globular features observed previously were now less pronounced. Thus, it appears that the PGalA diffused and adsorbed into the gaps between the PLL 7 nm dendrimer aggregates resulting in the lower RMS of the film surface. Transfer of the sample between the QCMD apparatus and the AFM, and back to the QCMD apparatus allowed further deposition to be monitored, provided the sample was not allowed to dry during transfer process. Subsequent deposition steps 5th layer (PLL 7 nm dendrimer) and 6th layer (PGalA), monitored by QCMD, exhibited similar deposition patterns (Fig. 6d and e). Deposition of the 5th (PLL 7 nm dendrimer) layer led to a significant decrease in $\Delta f_3/3$ of -110 Hz and negligible change in dissipation. The calculated hydrated mass of 1800 ng cm^{-2} corresponds to a film thickness of 16 nm (Fig. 7d), indicating adsorption of twice the amount of the hydrated mass, as seen for formation of the 3rd layer. The corresponding AFM image (Fig. 8d) revealed pronounced spherical features associated with the deposition of the PLL 7 nm dendrimer leading to a significant increase in surface roughness (RMS) to 14.88 nm: once again this suggests aggregation of the dendrimers rather than uniform coverage of the previous layer. The deposition of the 6th PGalA layer led to a further decrease of $\Delta f_3/3$ of ~ -45 Hz and an increase in dissipation of 3×10^{-6} (Fig. 6e). This corresponds to formation of a 12 nm film with a total hydrated mass of 1250 ng cm^{-2} (Fig. 7e), considerably higher when compared to values observed on formation of the 4th PGalA layer. Interestingly, the significantly higher amount of PGalA adsorbed also led to the disappearance of the spherical protrusions, as shown in Fig. 8e. This suggests the PGalA layer fills in the gaps between the PLL 7 nm aggregates and submerges these structures yielding a relatively flat layer.

The combined QCMD and AFM results demonstrated the value of performing QCMD and AFM measurements for each deposition step on the same mica-coated QCMD sensor. The QCMD data indicated that the PLL 7 nm dendrimer-PGalA multilayer growth followed a non-linear regime. Usually, non-linear multilayer growth is attributed to the diffusion of PLL within the film. AFM measurements provided important information regarding the topography, coverage and heterogeneity of the multilayers as they are formed. Clearly as the multilayer grows the film becomes increasingly heterogeneous: the surface roughness changes and seems to promote a non-uniform distribution of the two polymers within the film. This heterogeneity will affect the calculation of the film thickness. Increase of the surface roughness, as revealed by AFM measurements, would increase the active area for adsorption allowing more of the biopolymer to be adsorbed at the next deposition step.

4. Conclusions

It has been shown that through deposition onto mica discs inserted into a conventional QCMD it is possible to image monolayers and multilayers formed from biological polymers. Through use of mica-coated quartz crystals it has been possible to obtain simultaneous QCMD and AFM measurements of monolayer and multilayer deposition onto mica. This can be achieved through direct imaging of the structures formed on the mica-coated quartz crystals or through imaging of mica discs inserted in a second QCMD cell connected in series or parallel to the cell containing the mica-coated quartz crystal. QCMD measurements of adsorption onto mica and the surface of standard quartz crystals showed that the nature of the surface affected both the rate of adsorption and the level of adsorption onto the surfaces. In the case of the globular protein lysozyme the AFM images showed that monolayer coverage was incomplete accounting for variability in the adsorbed hydrated mass and calculated thickness of the layer. For lysozyme and the PLL–PGalA systems it was possible to image multilayers and multilayer formation, either simultaneously using additional mica discs, or on the same sample, using mica-coated quartz crystals. For the PLL dendrimer-PGalA multilayers the AFM revealed marked changes in surface topology during multilayer formation. Thus use of AFM provides new information on surface topology which needs to be considered in interpreting QCMD data, and will be important in understanding film structure and the mechanism of deposition. For studies of local changes in film structure due to environmental changes, or as the result of enzymatic action, it would be necessary to carry out direct *in situ* studies using both QCMD and AFM: such work will require development of a novel cell attachment for the AFM which will allow direct simultaneous studies on the same sample.

Acknowledgements

The research described in this paper was funded through the BBSRC responsive mode grant BBE0110041 and through the BBSRC strategic grant to the Institute. The authors wish to thank Tim Noel and Patrick Gunning for experimental assistance and discussions.

References

Alves, N. M., Picart, C., & Mano, J. F. (2009). Self assembling and crosslinking of polyelectrolyte multilayer films of chitosan and alginate studied by QCM and IR spectroscopy. *Macromolecular Bioscience*, *9*(8), 776–785.

Bieker, P., & Schonhoff, M. (2010). Linear and exponential growth regimes of multi layers of weak polyelectrolytes in dependence on pH. *Macromolecules*, *43*(11), 5052–5059.

Borovsky, B., Mason, B. L., & Krim, J. (2000). Scanning tunneling microscope measurements of the amplitude of vibration of a quartz crystal oscillator. *Journal of Applied Physics*, *88*(7), 4017–4021.

Bund, A., Schneider, O., & Dehnke, V. (2002). Combining AFM and EQCM for the in situ investigation of surface roughness effects during electrochemical metal depositions. *Physical Chemistry Chemical Physics*, *4*(15), 3552–3554.

Choi, K. H., Friedt, J. M., Frederix, F., Campitelli, A., & Borghs, G. (2002). Simultaneous atomic force microscope and quartz crystal microbalance measurements: Investigation of human plasma fibrinogen adsorption. *Applied Physics Letters*, *81*(7), 1335–1337.

Daikhin, L., Gileadi, E., Katz, G., Tsionsky, V., Urbakh, M., & Zagidulin, D. (2002). Influence of roughness on the admittance of the quartz crystal microbalance immersed in liquids. *Analytical Chemistry*, *74*(3), 554–561.

de Kerchove, A. J., & Elimelech, M. (2007). Formation of polysaccharide gel layers in the presence of Ca^{2+} and K^{+} ions: Measurements and mechanisms. *Biomacromolecules*, *8*(1), 113–121.

Garg, A., Heflin, J. R., Gibson, H. W., & Davis, R. M. (2008). Study of film structure and adsorption kinetics of polyelectrolyte multilayer films: Effect of pH and polymer concentration. *Langmuir*, *24*(19), 10887–10894.

Guillaume-Gentil, O., Zahn, R., Lindhoud, S., Graf, N., Voros, J., & Zambelli, T. (2011). From nanodroplets to continuous films: How the morphology of polyelectrolyte multilayers depends on the dielectric permittivity and the surface charge of the supporting substrate. *Soft Matter*, *7*(8), 3861–3871.

Halthur, T. J., Arnebrant, T., Macakova, L., & Feiler, A. (2010). Sequential adsorption of bovine mucin and lactoperoxidase to various substrates studied with quartz crystal microbalance with dissipation. *Langmuir*, *26*(7), 4901–4908.

Heim, L. O., & Johannsmann, D. (2007). Oscillation-induced static deflection in scanning force microscopy. *Review of Scientific Instruments*, *78*(1).

Hemmersam, A. G., Rechendorff, K., Besenbacher, F., Kasemo, B., & Sutherland, D. S. (2008). pH-dependent adsorption and conformational change of ferritin studied on metal oxide surfaces by a combination of QCM-D and AFM. *Journal of Physical Chemistry C*, *112*(11), 4180–4186.

Hook, F., Kasemo, B., Nylander, T., Fant, C., Sott, K., & Elwing, H. (2001). Variations in coupled water, viscoelastic properties, and film thickness of a Mefp-1 protein film during adsorption and cross-linking: A quartz crystal microbalance with dissipation monitoring, ellipsometry, and surface plasmon resonance study. *Analytical Chemistry*, *73*(24), 5796–5804.

Iwata, F., Kawaguchi, M., Aoyama, H., & Sasaki, A. (1997). Ultrasonic micromachining on Al thin film using atomic force microscopy combined quartz crystal resonator. *Thin Solid Films*, *302*(1–2), 122–126.

Johannsmann, D., Reviakine, I., Rojas, E., & Gallego, M. (2008). Effect of sample heterogeneity on the interpretation of QCM(-D) data: Comparison of combined quartz crystal microbalance/atomic force microscopy measurements with finite element method modeling. *Analytical Chemistry*, *80*(23), 8891–8899.

Jordan, J. L., & Fernandez, E. J. (2008). QCM-D sensitivity to protein adsorption reversibility. *Biotechnology and Bioengineering*, *101*(4), 837–842.

Kautek, W., Dieluweit, S., & Sahre, M. (1997). Combined scanning force microscopy and electrochemical quartz microbalance in situ investigation of specific adsorption and phase change processes at the silver/halogenide interface. *Journal of Physical Chemistry B*, *101*(14), 2709–2715.

Kesimer, M., & Sheehan, J. K. (2008). Analyzing the functions of large glycoconjugates through the dissipative properties of their absorbed layers using the gel-forming mucin MUC5B as an example. *Glycobiology*, *8*(6), 463–472.

Kett, P. J. N., Casford, M. T. L., Yang, A. Y., Lane, T. J., Johal, M. S., & Davies, P. B. (2009). Structural changes in a polyelectrolyte multilayer assembly investigated by reflection absorption infrared spectroscopy and sum frequency generation spectroscopy. *Journal of Physical Chemistry B*, *113*(6), 1559–1568.

Kim, D. T., Blanch, H. W., & Radke, C. J. (2002). Direct imaging of lysozyme adsorption onto mica by atomic force microscopy. *Langmuir*, *18*(15), 5841–5850.

Laos, K., Parker, R., Moffat, J., Wellner, N., & Ring, S. G. (2006). The adsorption of globular proteins, bovine serum albumin and beta-lactoglobulin, on poly-L-lysine-furcellaran multilayers. *Carbohydrate Polymers*, *65*(3), 235–242.

Lu, J. R., Swann, M. J., Peel, L. L., & Freeman, N. J. (2004). Lysozyme adsorption studies at the silica/water interface using dual polarization interferometry. *Langmuir*, *20*(5), 1827–1832.

Lundin, M., Elofsson, U. M., Blomberg, E., & Rutland, M. W. (2010). Adsorption of lysozyme, beta-casein and their layer-by-layer formation on hydrophilic surfaces: Effect of ionic strength. *Colloids and Surfaces B: Biointerfaces*, *77*(1), 1–11.

Macakova, L., Yakubov, G. E., Plunkett, M. A., & Stokes, J. R. (2010). Influence of ionic strength changes on the structure of pre-adsorbed salivary films. A response of a natural multi-component layer. *Colloids and Surfaces B: Biointerfaces*, *77*(1), 31–39.

Martin, S. J., Frye, G. C., Ricco, A. J., & Senturia, S. D. (1993). Effect of surface-roughness on the response of thickness-shear mode resonators in liquids. *Analytical Chemistry*, *65*(20), 2910–2922.

Messina, G. M. L., Satriano, C., & Marletta, G. (2009). A multitechnique study of preferential protein adsorption on hydrophobic and hydrophilic plasma-modified polymer surfaces. *Colloids and Surfaces B: Biointerfaces*, *70*(1), 76–83.

Pellenc, D., Bennett, R. A., Green, R. J., Sperrin, M., & Mulheran, P. A. (2008). New insights on growth mechanisms of protein clusters at surfaces: An AFM and simulation study. *Langmuir*, *24*(17), 9648–9655.

Richter, R. P., Berat, R., & Brisson, A. R. (2006). Formation of solid-supported lipid bilayers: An integrated view. *Langmuir*, *22*(8), 3497–3505.

Richter, R. P., & Brisson, A. (2004). QCM-D on mica for parallel QCM-D-AFM studies. *Langmuir*, *20*, 4609–4613.

Richter, R. P., & Brisson, A. R. (2005). Following the formation of supported lipid bilayers on mica: A study combining AFM, QCM-D, and ellipsometry. *Biophysical Journal*, *88*, 3422–3433.

Richter, R. P., Him, J. L. K., Tessier, B., Tessier, C., & Brisson, A. R. (2005). On the kinetics of adsorption and two-dimensional self-assembly of annexin A5 on supported lipid bilayers. *Biophysical Journal*, *89*(5), 3372–3385.

Rodahl, M., Hook, F., Krozer, A., Brzezinski, P., & Kasemo, B. (1995). Quartz-crystal microbalance setup for frequency and Q-factor measurements in gaseous and liquid environments. *Review of Scientific Instruments*, *66*(7), 3924–3930.

Rojas, E., Gallego, M., & Reviakine, I. (2008). Effect of sample heterogeneity on the interpretation of quartz crystal microbalance data: Impurity effects. *Analytical Chemistry*, *80*(23), 8982–8990.

Sauerbrey, G. (1959). Verwendung von Schwingquartzen zur Wagung dunner Schichten und zur Mikrowagung. *Zeitschrift für Physik*, *155*, 206–222.

Westwood, M., Noel, T. R., & Parker, R. (2010). The characterisation of polygalacturonic acid-based multilayer films using a quartz crystal microbalance, a dual polarization interferometer and a Fourier-transform infrared spectrometer. *Soft Matter*, *6*, 3302–3315.